JOURNAL OF THE AMERICAN CHEMICAL SOCIETY

Subscriber access provided by United Arab Emirates University | Libraries Deanship

Article

A Synthetic Oxygen Atom Transfer Photocycle from a Diruthenium Oxyanion Complex

Amanda R. Corcos, József S. Pap, Tzuhsiung Yang, and John F. Berry

J. Am. Chem. Soc., **Just Accepted Manuscript** • DOI: 10.1021/jacs.6b05942 • Publication Date (Web): 13 Jul 2016

Downloaded from http://pubs.acs.org on July 14, 2016

Just Accepted

"Just Accepted" manuscripts have been peer-reviewed and accepted for publication. They are posted online prior to technical editing, formatting for publication and author proofing. The American Chemical Society provides "Just Accepted" as a free service to the research community to expedite the dissemination of scientific material as soon as possible after acceptance. "Just Accepted" manuscripts appear in full in PDF format accompanied by an HTML abstract. "Just Accepted" manuscripts have been fully peer reviewed, but should not be considered the official version of record. They are accessible to all readers and citable by the Digital Object Identifier (DOI®). "Just Accepted" is an optional service offered to authors. Therefore, the "Just Accepted" Web site may not include all articles that will be published in the journal. After a manuscript is technically edited and formatted, it will be removed from the "Just Accepted" Web site and published as an ASAP article. Note that technical editing may introduce minor changes to the manuscript text and/or graphics which could affect content, and all legal disclaimers and ethical guidelines that apply to the journal pertain. ACS cannot be held responsible for errors or consequences arising from the use of information contained in these "Just Accepted" manuscripts.

ACS Publications

Journal of the American Chemical Society is published by the American Chemical Society. 1155 Sixteenth Street N.W., Washington, DC 20036

Published by American Chemical Society. Copyright © American Chemical Society. However, no copyright claim is made to original U.S. Government works, or works produced by employees of any Commonwealth realm Crown government in the course of their duties.

A Synthetic Oxygen Atom Transfer Photocycle from a Diruthenium Oxyanion Complex

Amanda R. Corcos,† József S. Pap,†,‡ Tzuhsiung Yang,† and John F. Berry*,†

† *Department of Chemistry, University of Wisconsin – Madison, 1101 University Ave., Madison, Wisconsin, 53706, USA*

ABSTRACT.

Three new diruthenium oxyanion complexes have been prepared, crystallographically characterized, and screened for their potential to photochemically unmask a reactive Ru–Ru=O intermediate. The most promising candidate, $Ru_2(chp)_4ONO_2$ (**4**, chp = 6-chloro-2-hydroxypyridinate), displays a set of signals centered around *m/z* = 733 amu in its MALDI-TOF mass spectrum, consistent with the formation of the $[Ru_2(chp)_4O]^+$ ($[$**6**$]^+$) ion. These signals shift to 735 amu in **4***, which contains ^{18}O-labeled nitrate. EPR spectroscopy and headspace GC-MS analysis indicate that $NO_2^{\bullet}$ is released upon photolysis of **4**, also consistent with the formation of an $Ru_2(chp)_4O$ species. Photolysis of **4** in CH_2Cl_2 at room temperature in the presence of excess PPh_3 yields $OPPh_3$ in 173% yield; control experiments implicate $Ru_2(chp)_4O$ (**6**), $NO_2^{\bullet}$, and free NO_3^- as the active oxidants. Notably, $Ru_2(chp)_4Cl$ (**3**) is recovered after photolysis. Since **3** is the direct precursor to **4**, the results described herein constitute the first example of a synthetic cycle for oxygen atom transfer that makes use of light to generate a putative metal oxo intermediate.

INTRODUCTION.

The use of light in chemical synthesis is a topic of significant current interest.[1] We[2] and others[3] have recently used light to access putative, highly reactive transition metal-containing intermediates. The most well-known examples are metal nitride compounds (**I**), which can be photochemically accessed from metal azide precursors (Scheme 1).[4] Metal terminal oxo species (**II**) are related reactive intermediates that are of great importance for biological and synthetic oxidation reactions.[5] Typically, chemical or electrochemical redox reactions[5a,6] are used to access **II**, but here we probe the possibility of photochemically unmasking a highly reactive species **II**, as in the bottom of Scheme 1.

Scheme 1. Formation of mononuclear metal nitride and oxo species after exposure of metal azides and oxyanions to light, respectively.

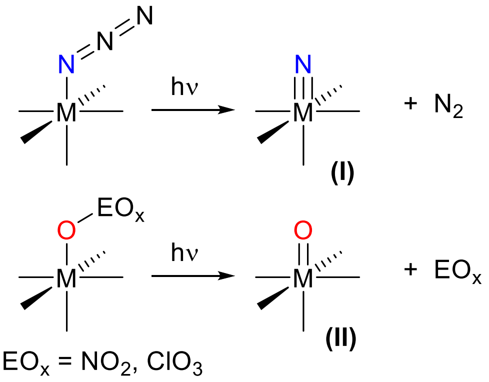

Important precedents for this work include the elimination of nitrite ion from an O=Ru–ONO_2 complex to produce a dioxo Ru species[7] and disproportionation of nitrite to form both Ru=O and Ru–NO complexes.[8] Furthermore, Suslick[9] and Vogler[10] have reported formation and reactivity of metal oxo species by photolytic cleavage of complexes with O-coordinated oxyanions, while Newcomb[11] and Bakac[12] have used flash photolysis to observe similar, highly reactive species. A major difficulty hindering the synthetic utility of this approach is the question of how to regenerate the M–OEO_x precursor (Scheme 2). This transformation, shown with a question mark in Scheme 2, is problematic because substrate (S) oxidation yields a coordinatively unsaturated metal complex that is reduced by one-electron from the original M–OEO_x species. Installation of OEO_x^- with concomitant one-electron oxidation is problematic because the OEO_x^- ions themselves can act as two-electron oxidants. We report here a solution to this problem that makes use of the properties of metal-metal bonded compounds.

Scheme 2. Possible stoichiometric cycle illustrating the synthetic limitations of current oxyanion systems.

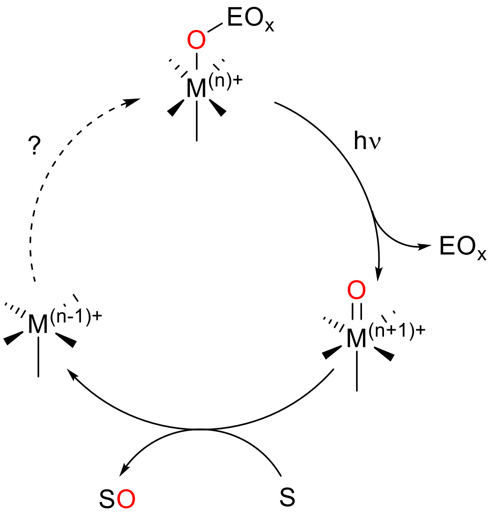

We recently described the first examples of M–M=O species (in which M = Mo or W) and we found them to display unusual reactivity.[13] Related Ru–Ru=O intermediates have recently been proposed to be important in sulfide oxygenation[14] and water oxidation[15] catalysis; furthermore, Ru_2(II/II) complexes have been shown to reversibly bind O_2.[16] Putative Ru–Ru=O species are highly reactive and have not been observed or isolated. Due to their important catalytic applications and our previous expertise in the chemistry of Ru–Ru≡N intermediates, we sought to use the photochemical methods outlined above to access Ru–Ru=O species in order to explore their fundamental reactivity. We also find the Ru–Ru=O species to be unstable, but it can nonetheless be utilized in a synthetic photocycle for oxygen atom transfer.

RESULTS AND DISCUSSION.

To date, only two discrete (non-polymeric) Ru_2 compounds bearing axial oxyanionic ligands are known: $Ru_2(DMBA)_4(ONO_2)_2$ (DMBA = *N,N'*-dimethylbenzamidinate),[17] which contains two η^1-coordinated nitrate ligands, and $Ru_2(OAc)_4(ONO_2)(H_2O)$,[18] which forms polymeric chains upon loss of the aquo ligand. We are instead keen to explore whether a discrete, anhydrous mono-oxyanion complex with an Ru–Ru–O–EO_x structure could be prepared. As such we turned to the DPhF (DPhF = *N,N'*-diphenylformamidinate) and chp (chp = 6-chloro-2-hydroxypyridinate) ligands, for their steric bulk near the axial coordination site should eliminate the possibility of forming polymeric chains and only one oxyanionic ligand should bind to the Ru_2 core based on charge balance. The compounds discussed herein are given in Chart 1.

Chart 1. Compounds discussed herein.

Entry	Complex	Ligands
1	$Ru_2(DPhF)_4Cl$	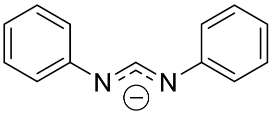 DPhF
2	$[Ru_2(DPhF)_4][NO_3]$	
3	$Ru_2(chp)_4Cl$	
4	$Ru_2(chp)_4ONO_2$	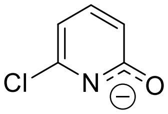 chp
5	$Ru_2(chp)_4OClO_3$	

Synthesis and IR Spectroscopic Characterization. Compounds **2**, **4**, and **5** were prepared from the chloride precursors **1** and **3** by metathesis with the appropriate Ag^+ salts ($AgNO_3$ for **2** and **4**; $AgClO_4$ for **5**) as seen in Scheme 3. The IR spectrum for **2** displays a signal at 1773 cm^{-1}, which is well within the characteristic range of 1700-1800 cm^{-1} for free nitrate anions.[19] Furthermore, the MALDI-TOF mass spectrum of **2** shows an isotopic envelope indicative of the free $[Ru_2(DPhF)_4]^+$ core (Figure S1), and the crystal structure of **2** consists of well-separated $[Ru_2(DPhF)_4]^+$ cations and NO_3^- anions.[20] The steric bulk of the DPhF phenyl rings therefore prevents NO_3^- coordination. In contrast, the IR spectra of **4** and **5** display signals consistent with O-coordinated nitrate[19b] and perchlorate ligands[19b,21] (1278 cm^{-1} [ν_{asym} (ONO)] for **4**; ν_4 = 1154, 1134, 1025 cm^{-1}, and ν_2 = 894 cm^{-1} for **5**).

Scheme 3. Formation of nitrate complex **2** from chloride precursor **1** and oxyanion complexes **4** and **5** from chloride precursor **3**.

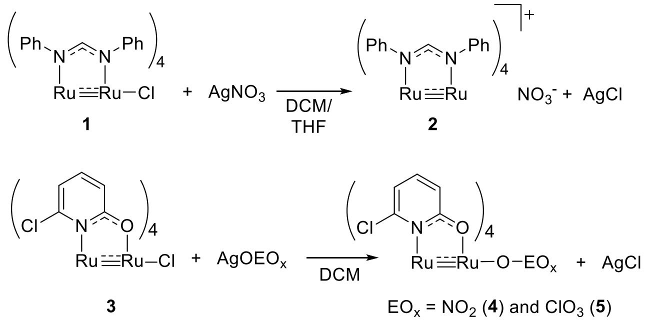

Crystallography. Compounds **4** and **5** have been characterized by X-ray crystallography (Figures 1, 2 and Table S1). As with the chloride precursor **3**[22] and azide analog $Ru_2(chp)_4N_3$,[2d] the equatorial chp ligands in **4** and **5** are bound in a (4,0) orientation, which allows for the oxyanionic ligand to bind only to the exposed Ru axial site.

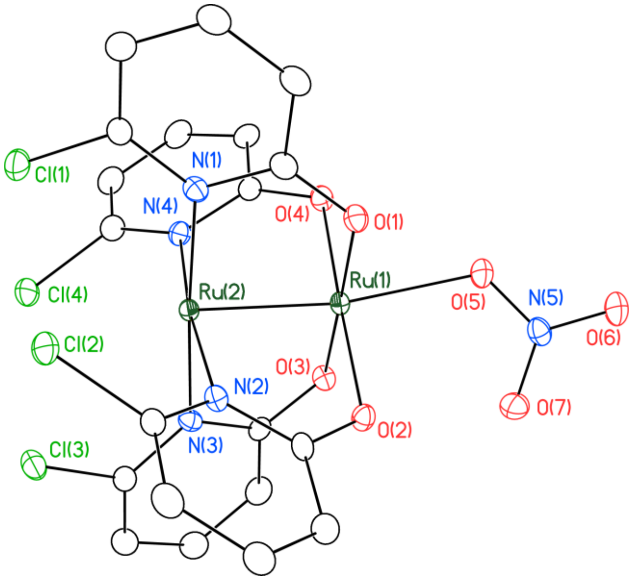

Figure 1. Thermal ellipsoid plot of **4**·$2CH_2Cl_2$ with ellipsoids drawn at the 50% probability level. Hydrogen atoms and molecules of solvation are omitted for clarity.

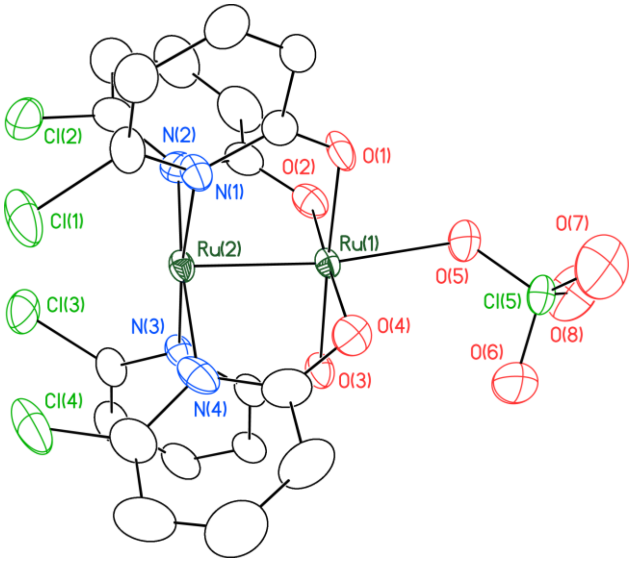

Figure 2. Thermal ellipsoid plot of **5**·$2CH_2Cl_2$ with ellipsoids drawn at the 50% probability level. Hydrogen atoms and molecules of solvation are omitted for clarity.

The Ru–Ru distances in **4** and **5** (2.2633(3) Å and 2.2540(7) Å,[23] respectively, listed in Table 1) are in accord with all other previously characterized Ru_2^{5+} oxypyridinate complexes.[24]

The Ru(2)–Ru(1)–O(5) bond angle in **4** deviates from linearity to 170.07(7)° and that in **5** deviates to 170.9(2)°, likely due to crystal packing effects. At 1.221(3) Å and 1.236(3) Å, the nitrate N–O distances (N(5)–O(6) and N(5)–O(7), respectively) in **4** are slightly shorter than, but in line with, those of an unbound nitrate anion (1.241(2) Å).[25] At 1.306(3) Å, the O(5)–N(5) distance is significantly longer, causing the nitrate anion to lose 3-fold symmetry due to the Ru(1)–O(5) interaction. The O(6)–N(5)–O(7) angle is 122.1(3)° and, when combined with the other O–N–O angles (118.4(3)° and 119.4(2)°), sum to 359.9°, indicating a planar nitrate group, which is oriented parallel to the Ru–Ru bond. The perchlorate anion in **5** exhibits O–Cl–O angles that range from 107.0(3)° – 112.8(4)°, which are close to the idealized geometry of 109.5° for a tetrahedral anion. The O(5)–Cl(5) distance is slightly elongated at 1.464(4) Å compared to the other O–Cl bond distances of 1.370(5) Å, 1.392(5) Å, and 1.445(6) Å.

Table 1. Selected crystallographic bond lengths and angles for **4** and **5**. E = N for **4**, Cl for **5**.

Compound	**4**	**5**
Ru(1)–Ru(2) Å	2.2633(3)	2.2540(7)
Ru(1)–O(5) Å	2.200(2)	2.249(4)
O(5)–E(5) Å	1.306(3)	1.464(4)
E(5)–O(6) Å	1.221(3)	1.445(6)
E(5)–O(7) Å	1.236(3)	1.370(5)
E(5)–O(8) Å	–	1.392(5)
Ru(2)–Ru(1)–O(5) (°)	170.07(6)	170.9(2)

UV/Vis Spectroscopy. The most intense absorption feature for compounds **3-5** in CH_2Cl_2 shifts from 529 to 532 to 542 nm and increases in intensity as the coordinating strength of the anion increases (**5** < **4** < **3**) (Figure 3). Though this electronic transition has not been definitively assigned, the variation in energy and intensity observed here suggests that it has significant LMCT character involving the axial ligand. The secondary feature in the spectrum also shifts from 666 to 678 to 689 nm in the same manner (**5** < **4** < **3**), but the intensity of this feature remains relatively consistent throughout the series.

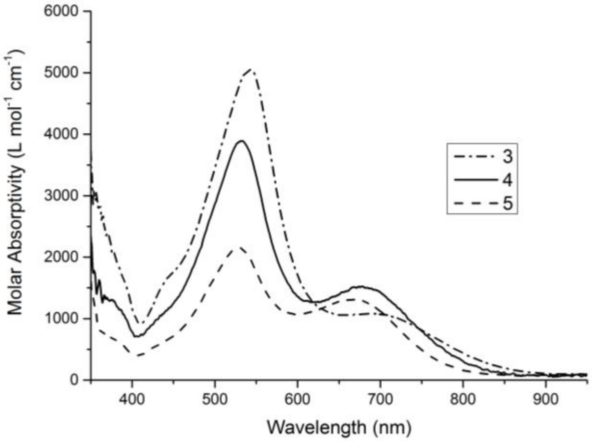

Figure 3. UV/Vis for compounds **3-5** in CH_2Cl_2. The spectrum for **3** was previously reported[22] but is included here for direct comparison.

Cyclic Voltammetry. Cyclic voltammograms of **4** and **5** were recorded under two distinct sets of conditions. Solutions of **3-5** in CH_2Cl_2 with 0.1 M NBu_4PF_6 electrolyte were examined, as well as solutions of **4** in 0.1 M NBu_4NO_3 and **5** in 0.1 M NBu_4ClO_4. These varying conditions give insight into the binding of NO_3^- and ClO_4^- anions to the $[Ru_2(chp)_4]^+$ core in solution. In analyzing these data, we can consider two limiting cases. If, first, the NO_3^- and ClO_4^- anions dissociate completely from **4** and **5** in CH_2Cl_2, then we would expect both compounds to have identical CV traces in 0.1 M NBu_4PF_6. If, on the other hand, we assume that NO_3^- and ClO_4^- do not dissociate at all from **4** or **5** in solution, then we would expect the CV traces of **4** with NBu_4PF_6 and NBu_4NO_3 electrolytes to be identical, and the CV traces of **5** with NBu_4PF_6 and NBu_4ClO_4 to be identical as well. The data shown in Figure 4 (see also Table 2) show clearly that neither of these limiting cases reflects reality. The fact that the CVs of **4** and **5** in NBu_4PF_6

appear distinct indicates that these solutions do not simply contain free $[Ru_2(chp)_4]^+$ cations. However, the fact that the redox potentials change when the electrolyte is changed to NBu_4NO_3 or NBu_4ClO_4 indicates that both **4** and **5** undergo the following equilibrium in solution: $Ru_2(chp)_4X \rightleftharpoons [Ru_2(chp)_4]^+ + X^-$. Other diruthenium compounds show similar behavior.[26] Addition of excess X^- shifts this equilibrium to the left. This is clearly a fast equilibrium relative to the timescale of the electrochemical measurement since we do not observe distinct waves that may be assigned to $Ru_2(chp)_4X$ and $[Ru_2(chp)_4]^+$. These results indicate that both $Ru_2(chp)_4X$ species and free X^- are chemically relevant on the timescale of photolysis experiments in fluid solution at room temperature (vide infra).

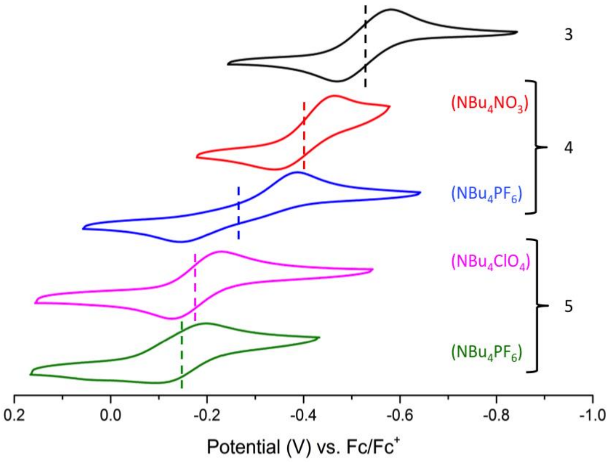

Figure 4. Cyclic voltammograms of $Ru_2^{5/4+}$ couple for **3-5** versus Fc/Fc^+. $E_{1/2}$ for each species is marked with a dashed vertical line.

Table 2. E values for $Ru_2^{5/4+}$ couple for **1-5** vs. Fc/Fc^+ in CH_2Cl_2 with scan rate = 100 mV/s. Electrolyte is 0.1 M. *Indicates quasi-reversible. $^\#$Previously reported against SCE[26b] and converted here to be against Fc/Fc^+.[27] ‡Previously reported against Ag/AgCl[28] and re-measured here for direct comparison.

Compound	Electrolyte	$E_{1/2}$ (V)	E_c (V)	E_a (V)
1		–	-1.1$^{\#}$	–
2	NBu_4PF_6	-0.687	–	–
3	NBu_4PF_6	-0.525‡	-0.581	-0.469
4	NBu_4NO_3	-0.401*	-0.465	-0.338
4	NBu_4PF_6	-0.267*	-0.388	-0.146
5	NBu_4ClO_4	-0.179*	-0.230	-0.127
5	NBu_4PF_6	-0.145*	-0.197	-0.094

Photolysis Screening by Mass Spectrometry. MALDI-TOF mass spectrometry is a particularly useful method for screening photolytically-active compounds. In this case, the MALDI-TOF nitrogen laser (337 nm) is the light source, and photolysis products can be directly observed in the mass spectrum. The most prominent set of signals for **4** and **5** in MALDI-TOF mass spectrometry experiments corresponds to the $Ru_2(chp)_4^+$ core with the characteristic Ru_2 isotopic distribution centered around m/z = 717 amu (Figure 5 for **4**; Figure S2 for **5**), indicating facile loss of the axially-bound oxyanions. In the case of **4**, there is a weak Ru_2 signal centered at m/z = 733 amu, which is consistent with an $[Ru_2(chp)_4O]^+$ ion, suggesting that an Ru_2O species could be formed upon photolysis of **4**. This is also similar to the case of Ru_2-azide compounds that show Ru_2N signals in their mass spectra due to photolysis.[2] To further support this hypothesis, we used labeled ^{18}O-nitrate ($N^{18}O_3^-$) to form $Ru_2(chp)_4{}^{18}ON^{18}O_2$ (**4***), and we found that the Ru_2O feature shifts in the mass spectrum to m/z = 735 amu (Figure 5). This shift clearly indicates that the axial O atom in the $[Ru_2(chp)_4O]^+$ ion derives from nitrate and is fully consistent with photo-dissociation of $NO_2^\bullet$ or NO_2^- from **4**. The m/z = 733 amu feature is present but barely discernable in the spectrum of **5** (Figure S2), suggesting to us that perchlorate may not be as suitable a precursor for the formation of an Ru_2O intermediate. Therefore only **4** was investigated further.

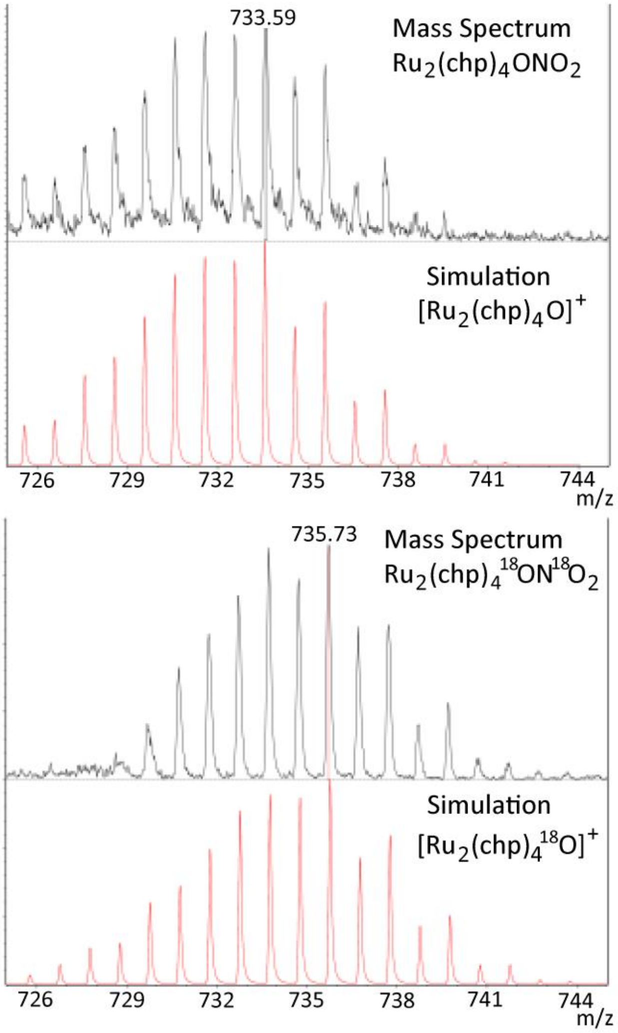

Figure 5. MALDI-TOF mass spectrum for **4** (black, top). Simulation (red) indicates isotope pattern at *m/z* = 733 amu is due to $[Ru_2(chp)_4O]^+$. Upon isotopic labeling, MALDI-TOF mass spectrum for **4*** (black, below) shifts by 2 units, as confirmed by simulation (red, bottom).

In photolysis experiments of **4** there are two possible sites at which bonds could break homolytically: (a) the Ru–ONO_2 bond or (b) the RuO–NO_2 bond (Scheme 4). Previous studies have indicated that either site is possible.[11a,11b,29] Heterolytic RuO–NO_2 bond cleavage is another possible pathway (pathway c in Scheme 4), which has been demonstrated for perchlorate compounds.[11b] Both pathways b and c would explain our mass spectrometry results. Upon homolysis (pathway b), the resulting radical species $NO_2^\bullet$ should be EPR active, unlike its Ru_2O counterpart $Ru_2(chp)_4O$ (**6**), which is anticipated to have a ground state of $S = 0$.[30] Heterolysis (pathway c), on the other hand, would give rise to an EPR-active Ru_2O^+ species. Thus, we decided to use EPR spectroscopy to assess the mechanism of photolysis for **4**.

Scheme 4. Possible products upon exposing nitrate complexes to photolytic conditions.

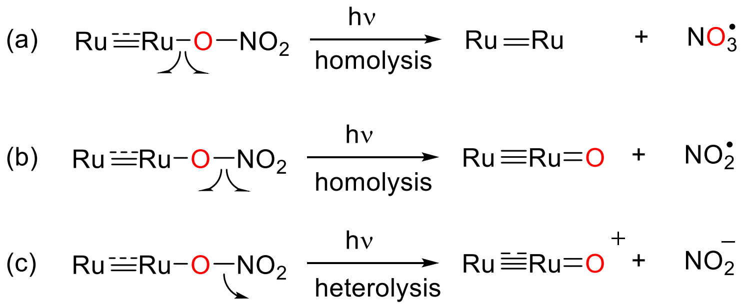

*Photolysis of **4** in Frozen Solution at 77 K and in Fluid Solution at Room Temperature.* The EPR spectra of **2**, **4**, and **5** (Figures S3, 6, and S4, respectively) were measured at 10 or 15 K in a frozen solution of CH_2Cl_2. Though electrochemical measurements (vide supra) suggest the presence of an equilibrium between Ru_2–bound and –unbound nitrate species, the 10 K EPR spectrum of **4** can be modeled with a single axial signal, with effective *g* values of 3.86 and 1.95, consistent with an $S = 3/2$ ground state where D >> hν (Table 3). Thus, the nitrate-bound **4** is most likely the dominant species in solution at this temperature, and its prominent EPR signal can be used to assess the efficacy of photolysis of **4** in frozen solution.

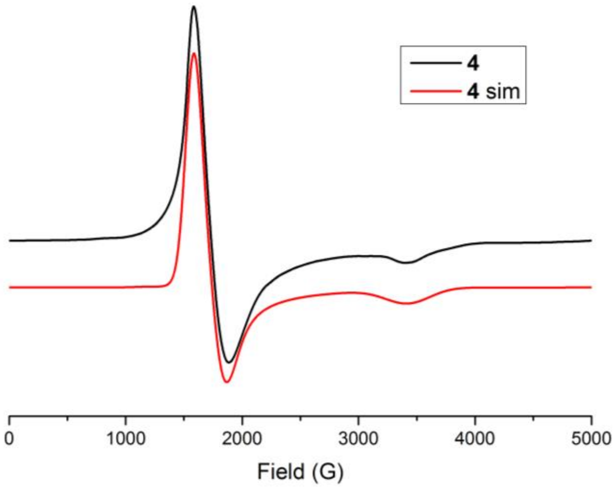

Figure 6. EPR spectrum and simulation of **4** recorded at 10 K.

Table 3. EPR spectral simulations for **2**, **4**, and **5**.

Compound	**2**	**4**	**5**
$g_{\perp}$	2.125	2.01	2.00
$g_{\|}$	1.94	1.95	1.93
E/D	0.006	0.035	0.033
HStrain[a]	850, 350, 450	1200, 900, 1200	1550, 850, 1100

[a] HStrain accounts for anisotropic line broadening due to unresolved hyperfine coupling

Exposure of a frozen CH_2Cl_2 solution of **4** to 350 nm wavelength light at 77 K for 8 hours yields no change in the intensity of the EPR signal of **4**. Switching to 254 nm light and photolyzing for 16 hours at 77 K yields the EPR spectrum shown in Figure 7. There is a slight decrease in the signal intensity from the *S* = 3/2 signal of **4** and, more significantly, a new feature in the *g* = 2 region is present. This new signal is an isotropic 1:1:1 triplet, clearly indicating a radical species with hyperfine coupling involving an *I* = 1 ^{14}N nucleus, and it compares favorably to known literature values for $NO_2^{\bullet}$ versus those of $NO_3^{\bullet}$ (Figure 7, inset).[31] The presence of

$NO_2^\bullet$ suggests that, though photolysis of **4** proceeds in low yield at 77 K, homolytic cleavage of the O(5)–N(5) nitrate bond is the primary photolysis pathway (pathway b in Scheme 4).

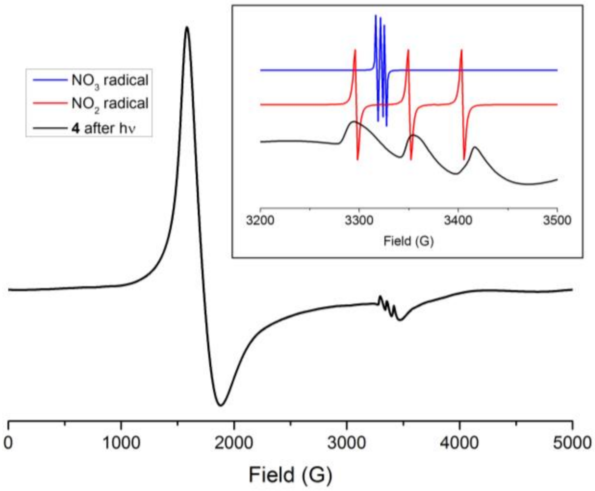

Figure 7. EPR spectrum of **4** in CH_2Cl_2 taken at 10 K after 16 hours of frozen photolysis using 254 nm light. Inset: simulations[31] of $NO_3^\bullet$ (blue, above) and $NO_2^\bullet$ (red, middle) compared to **4** after frozen photolysis (black, below).

In order to improve the yield of photolysis, subsequent experiments were performed on fluid solutions of **4** in CH_2Cl_2 at room temperature under N_2. Under these conditions, photolysis is complete in a shorter time period of 4 hours using 350 nm wavelength light. Using the isotopically-enhanced analog **4***, GC-MS analysis of the headspace of the reaction confirms formation of $N^{18}O_2^\bullet$ (m/z = 50) in significant quantities (Figure 8), further supporting the homolytic cleavage mechanism (pathway b in Scheme 3) suggested by our EPR results.

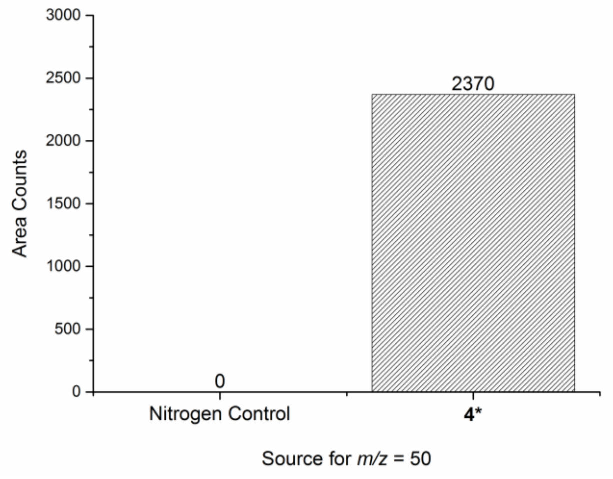

Figure 8. GC-MS headspace analysis for the formation of $N^{18}O_2^{\bullet}$ ($m/z = 50$) after photolysis of **4*** at room temperature under N_2 for 4 hours using 350 nm wavelength light. As compared to the counts for $m/z = 50$ amu for the N_2 control, $N^{18}O_2^{\bullet}$ is clearly formed under reaction conditions.

*Oxygen Atom Transfer via Room Temperature Photolysis of **4***. Room temperature fluid solution photolytic experiments were also performed in the presence of an excess of the well-known oxygen atom acceptor PPh_3 and monitored for the formation of oxygen atom transfer products. A CH_2Cl_2 solution of **4** and PPh_3 (20 eq. vs. **4**) was photolyzed for 4 hours using 350 nm light at room temperature under N_2. Analysis by $^{31}P\{^1H\}$ NMR spectroscopy indicates the formation of the intermolecular oxygen atom transfer product $OPPh_3$ in > 100% yield (determined by ^{31}P NMR integration against a standard of PPh_4Cl) (Figure 9). The identity of this product was confirmed by doping with an authentic sample of $OPPh_3$ (Figure S5) and is further corroborated by ESI mass spectral data, which shows that the product formed in this reaction with **4** has a mass of $m/z = 279$ amu (consistent with $OPPh_3$) (Figure S6) and shifts by 2 mass units to $m/z = 281$ amu (consistent with $^{18}OPPh_3$) upon using **4*** (Figure S7).

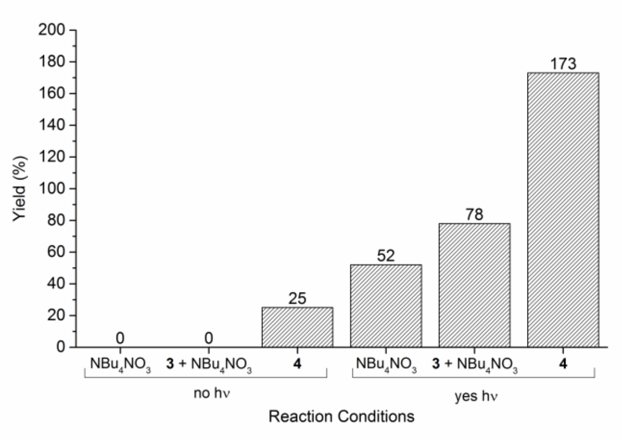

Figure 9. Yield of $OPPh_3$ after exposure to different oxygen atom sources, both with and without exposure to photolytic conditions.

The > 100% yield of $OPPh_3$ implies that more than one active oxidant is formed under these conditions. As mentioned above, some amount of free NO_3^- is expected to be present based on our electrochemistry results. Upon UV irradiation at ~ 300 nm, unbound nitrate is known to eliminate either ^3P O or O^- [32] or to isomerize to peroxynitrite.[33] To test the possibility that unbound nitrate is the sole oxygen atom source, photolysis of NBu_4NO_3 was performed under identical conditions as previously expressed. $OPPh_3$ is indeed generated but in less than one-third the yield as when **4** was used (Figure 9). We also considered the possibility that the Ru_2 complex could simply act as a photosensitizer for free NO_3^-. A control reaction was therefore performed in which NBu_4NO_3 and PPh_3 were photolyzed in the presence of $Ru_2(chp)_4Cl$ (**3**) as a photo-sensitizer (Figure 9). $OPPh_3$ is generated in better yields here than without **3**, but this result still does not match our findings with **4**. Therefore, $OPPh_3$ can be formed from free NO_3^- anion but is formed more efficiently from **4**.

It is conceivable that O_2 could be formed from either nitrate photolysis or bimetallic reductive coupling of Ru_2O intermediates and could be the oxygen atom source for formation of

$OPPh_3$. To test this possibility, **4*** was photolyzed in a CH_2Cl_2 solution at room temperature and analysis of the reaction headspace was performed using GC-MS. These results indicate that $^{18}O_2$ is not formed (Figure S8). Another potential oxygen atom source is the photolysis byproduct $NO_2^{\bullet}$.[9b,10] To probe this possibility, PPh_3 was exposed to $NO_2^{\bullet}$. ESI mass spectrometry data indicate that the resulting product is indeed $OPPh_3$ (Figure S9). To see whether $NO_2^{\bullet}$ is fully consumed under our reaction conditions, **4** was photolyzed in a CH_2Cl_2 solution containing 20 equivalents of PPh_3 at room temperature, and analysis of the reaction headspace was performed using GC-MS (Figure S10). Free $NO_2^{\bullet}$ is still detected under these conditions, though in smaller yields than without PPh_3 present. Thus $NO_2^{\bullet}$ is likely to be an oxygen atom source in this system but clearly cannot be the sole source. We therefore propose that the oxygen atom transfer in this system derives from three active oxidants: free nitrate ion, $NO_2^{\bullet}$, and an Ru–Ru=O intermediate, giving yields of $OPPh_3$ greater than 100%.

Finally, we were interested in determining the identity of the resulting Ru_2 species after completion of room temperature photolysis in the presence of PPh_3. Only one Ru_2 product was observed and isolated. MALDI-TOF mass spectrometry and UV/Vis confirm this product to be the precursor **3**. This result was surprising to us since oxygen atom transfer from an Ru–Ru=O species should yield an Ru_2(II/II) product such as $Ru_2(chp)_4PPh_3$, a species that we have recently characterized.[34] However, low-valent metal-metal bonded dimers are known to react with light and halogenated solvents to yield one-electron oxidized compounds bearing an axial halide ligand.[35] This reaction sequence explains the formation of **3**, as shown in Scheme 5. As emphasized by Scheme 5, our results present a complete synthetic photocycle for oxygen atom transfer from a photoactive oxyanion complex.

Scheme 5. Proposed mechanistic scheme for the oxygen atom transfer reaction presented here. Proposed intermediates **6** and $Ru_2(chp)_4$ are in dashed boxes.

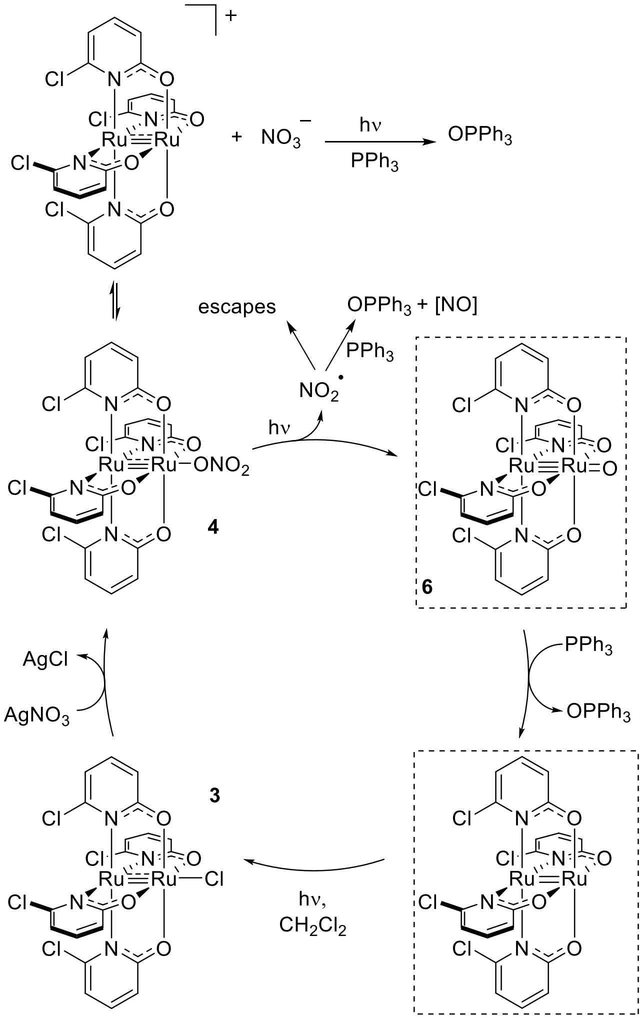

CONCLUSIONS.

Whereas the $[Ru_2(DPhF)_4]^+$ core is not sterically accessible to bind non-linear anions as ligands, the $[Ru_2(chp)_4]^+$ core does support the formation of discrete, mono-oxyanion complexes with η^1-nitrate and -perchlorate anions. Mass spectrometry, EPR, and GC-MS analysis data suggest that photolysis of **4** proceeds to generate Ru–Ru=O species **6** and $NO_2^•$. Room temperature photolysis of **4** allows for oxygen atom transfer to PPh_3 to form $OPPh_3$ in a synthetic photocycle that regenerates **3**. We therefore propose that PPh_3 is directly oxidized by a combination of three active oxidants: photosensitized NO_3^-, reactive intermediate **6**, and additionally by $NO_2^{\bullet}$. This work demonstrates for the first time that the generation of a reactive metal oxo species from an oxyanion complex can be incorporated into a synthetic cycle. Further exploitation of these reaction conditions, along with efforts to stabilize and characterize the putative Ru–Ru=O intermediate are underway in our lab.

EXPERIMENTAL SECTION.

General Methods. All syntheses were conducted under a dry N_2 atmosphere using Schlenk line techniques unless otherwise noted; product workup and isolation were achieved in air unless otherwise noted. Dichloromethane (CH_2Cl_2) was dried with CaH_2 and distilled before use. Hexanes were obtained from a Vacuum Atmospheres Solvent System and degassed prior to use. All materials were commercially available and used as received, unless otherwise noted. Compounds **1**[26b,36] and **3**[2d,22] were prepared according to literature procedures. Photolysis of frozen samples of **4** were performed in a Rayonet RPR-200 photochemical reactor with light from 254 and 350 nm mercury vapor lamps.

*$[Ru_2(DPhF)_4][NO_3]$ (**2**).* $Ru_2(DPhF)_4Cl$ (200 mg, 0.196 mmol, 1 eq.) was dissolved in CH_2Cl_2 and added to a suspension of $AgNO_3$ (500 mg, 2.94 mmol, 15 eq.) in 3 mL of THF in air. The color of the mixture changed from green to purple-blue almost instantaneously and was allowed to continue stirring at RT overnight. The solids were filtered off and the remaining solution was left to evaporate slowly to yield dark purple crystals of the product. Yield: 180 mg, 87.7%. MW: 1045.10 g mol^{-1}. MALDI-TOF (m/z): ($[M - NO_3]^+$) 984. IR (ATR): 3053, 1773 [ν_{sym} NO_3], 1591, 1520, 1486, 1449, 1364, 1349, 1314, 1214, 1175, 1156, 1078, 1027, 936, 827, 761, 693,

668, 658, 619. UV-Vis (CH_2Cl_2):. $\lambda_{max}(\varepsilon)$ = 437 (4250), 527 (5950), 681 (7170 mol^{-1} L cm^{-1}). [$C_{52}H_{44}N_9O_3Ru_2 \cdot CH_2Cl_2 \cdot 2H_2O$]: calcd. C 54.59, H 4.32, N 10.81; found C 54.31, H 3.88, N 11.37. Crystals suitable for X-ray diffraction were grown via slow evaporation from a concentrated solution of CH_2Cl_2 at room temperature.

*$Ru_2(chp)_4ONO_2$ (**4**).* $Ru_2(chp)_4Cl$ (200.0 mg, 0.266 mmol, 1 eq.) and $AgNO_3$ (54.6 mg, 0.321 mmol, 1.2 eq.) were dissolved in 30 mL of freshly distilled CH_2Cl_2 and allowed to stir for 96 h at RT under static N_2. A white precipitate (AgCl) formed. The reaction mixture was filtered through a fine sintered glass frit. Excess CH_2Cl_2 was washed through the frit until it was no longer colored. The filtrate was removed under reduced pressure, and the resulting purple solid was washed with hexanes and collected. Yield: 195.5 mg, 94.4%. MW: 778.29 g mol^{-1}. MALDI-TOF (m/z): ($[M - NO_2]^+$) 733, ($[M - ONO_2]^+$) 717. IR (ATR): 3108, 2964, 1596, 1534, 1465, 1434, 1390, 1350, 1278 [ν_{asym} (ONO)], 1262, 1181, 1085, 1011, 964, 942, 931, 866, 795, 789, 724, 630 cm^{-1}. UV-Vis (CH_2Cl_2): $\lambda_{max}(\varepsilon)$ = 532 (3890), 678 (1520 mol^{-1} L cm^{-1}). [$C_{20}H_{12}Cl_4N_5O_7Ru_2$]: calcd. C 30.86, H 1.55, N 8.99; found C 30.64, H 1.44, N 8.81. Crystals suitable for X-ray diffraction were grown from a saturated CH_2Cl_2 solution at -80 °C.

*$Ru_2(chp)_4OClO_3$ (**5**).* $Ru_2(chp)_4Cl$ (200.0 mg, 0.266 mmol, 1 eq.) and $AgClO_4$ (66.7 mg, 0.322 mmol, 1.2 eq.) were dissolved in 30 mL of freshly distilled CH_2Cl_2 and allowed to stir for 96 h at RT under static N_2. A white precipitate (AgCl) formed. The reaction mixture was filtered through a fine sintered glass frit. Excess CH_2Cl_2 was washed through the frit until it was no longer colored. The filtrate was concentrated under reduced pressure, and the resulting purple solid was washed with hexanes and collected. Yield: 205.3 mg, 94.6%. MW: 815.74 g mol^{-1}.

MALDI-TOF (m/z): ([M – ClO_3]$^+$) 733, ([M – $OClO_3$]$^+$) 717. IR (ATR): 3107, 1596, 1536, 1433, 1391, 1337, 1263, 1154 [ν_4], 1134 [ν_4], 1075, 1025 [ν_4], 1013, 932, 894 [ν_2], 790, 723, 705, 668, 632, 610 cm^{-1}. UV-Vis (CH_2Cl_2): $\lambda_{max}(\varepsilon)$ = 529 (2150), 666 (1310 mol^{-1} L cm^{-1}). [$C_{20}H_{12}Cl_5N_4O_8Ru_2$]: calcd. C 29.45, H 1.48, N 6.87; found C 29.20, H 1.68, N 6.26. Crystals suitable for X-ray diffraction were grown from a saturated CH_2Cl_2 solution layered with hexanes at room temperature. *Safety warning: anhydrous metal perchlorate complexes are potentially explosive.*

$AgN^{18}O_3$. 0.1 g $HN^{18}O_3$ (95 atom %, 65 weight % in $H_2{}^{18}O$), 0.1 g $H_2{}^{18}O$, Ag powder, and a stir bar were added to a vial that was subsequently capped. This heterogeneous mixture was stirred at 50 °C in air for 48 hours; periodically the mixture was manually rotated and the solvent mixture forced to the bottom of the vial as it had crept up the walls of the vial. A white solid became visible as the reaction reached completion, which was re-dissolved in the $H_2{}^{18}O$. The supernatant liquid was then decanted away (using a pipette) from the heterogeneous solid mixture into a new vial and allowed to evaporate to dryness, leaving a crystalline product, which was dried under vacuum at 50 °C overnight. Yield: 126.8 mg (76.5%). IR (ATR): 1676, 1657 [ν_{asym} ($^{18}ON^{18}O$)], 1293 [ν_{sym} ($^{18}ON^{18}O$)], 792 [ν ($N^{18}O$)], 694 cm^{-1}.

*$Ru_2(chp)_4{}^{18}ON^{18}O_2$ (**4***).* $AgN^{18}O_3$ was ground into fine powder and then used in an identical procedure as **4**. Yield: 141.2 mg, 67.7%. MW: 784.29 g mol^{-1}. MALDI-TOF (m/z): ([M – $N^{18}O_2$]$^+$) 735. IR (ATR): 3108, 2964, 1596, 1534, 1465, 1434, 1390, 1350, 1253 [ν_{asym} ($^{18}ON^{18}O$)], 1262, 1181, 1085, 1011, 942, 931, 866, 795, 789, 724, 630 cm^{-1}.

Solution-phase Reactions. A 0.5 mM CH_2Cl_2 solution of the nitrate source (**4**, **3** + NBu_4NO_3, or NBu_4NO_3) with a 20-fold excess of PPh_3 was prepared on a 30 mL scale in a quartz Schlenk tube (flask "A"). A 10 mL aliquot was transferred to a different flask (flask "B"), which was wrapped in foil, and allowed to stir under static N_2 for 4 hours *without* exposure to photolytic conditions. The remaining 20 mL solution was photolyzed in flask "A" under static vacuum at room temperature using 350 nm light for 4 hours. After this time a 10 mL aliquot was removed and transferred to a 25 mL Schlenk flask (flask "C"). Solutions in flasks "B" and "C" were reduced to dryness under vacuum and analyzed by NMR with a known quantity (1 eq. based on **4**) of PPh_4Cl for use as a comparative standard. $^{31}P\{^1H\}$ NMR (298 K, 400 MHz, $CDCl_3$): δ 29 ($OPPh_3$), 23 (PPh_4Cl), –5.5 (PPh_3).

Physical Measurements. Matrix-assisted laser desorption/ionization (MALDI) time-of-flight (TOF) mass spectrometry data were obtained using an anthracene matrix on a Bruker ULTRAFLEX® III mass spectrometer equipped with a SmartBeam® laser in positive ion detection mode. ESI mass spectrometry data was collected on a Thermo Q Exactive Plus™ mass spectrometer and GC-MS data were collected on a Shimadzu GCMS-QP2010 Ultra spectrometer. ^1H and $^{31}P\{^1H\}$ data were obtained using a Bruker Avance III 400 MHz spectrometer. UV/Vis spectra were obtained using a StellarNet Miniature BLUE-wave UV-Vis dip probe with a Tungsten-Krypton light source and a 10 mm path length tip. IR spectra were taken on a Bruker Tensor 27 spectrometer using an ATR adapter (no matrix). Cyclic voltammograms were taken on a BASi Potentiostat using Epsilon software in CH_2Cl_2 solutions with 0.1 M electrolyte and 1.0 mM substrate. The electrodes were as follows: glassy carbon (working), Pt wire (auxiliary) and Ag/Ag^+ in CH_3CN (reference). The potentials were referenced versus the ferrocene/ferrocenium redox couple by externally added ferrocene. Elemental analysis was performed by Midwest Microlab, LLC in Indianapolis, IN, USA.

EPR Spectroscopy. EPR data were acquired on a Bruker ELEXSYS E500 EPR spectrometer equipped with a Varian E102 microwave bridge interfaced with a Linux system. An Oxford Instruments ESR-900 continuous-flow helium flow cryostat and an Oxford Instruments 3120 temperature controller were used to control the sample temperature. A Hewlett-Packard 432A power meter was used for microwave power calibration, with measurement conditions as follows: for **2** – 9.3762 GHz, 4 G modulation amplitude, 2500 G center field, 5000 G sweep width, 5.024 mW power, 55 dB gain, 327.68 ms time constant, 10 ms conversion time, and 15 K; for **4** – 9.3765 GHz, 4 G modulation amplitude, 2500 G center field, 5000 G sweep width, 5.024 mW power, 60 dB gain, 655.36 ms time constant, 10 ms conversion time, and 10 K; for **4-**hν/$NO_2^{\bullet}$ – 9.3765 GHz, 4 G modulation amplitude, 2500 G center field, 5000 G sweep width, 5.024 mW power, 60 dB gain, 655.36 ms time constant, 10 ms conversion time, and 10 K; for **5** – 9.3832 GHz, 4 G modulation amplitude, 2500 G center field, 5000 G sweep width, 5.024 mW power, 55 dB gain, 655.36 ms time constant, 10 ms conversion time, and 10 K. Spectral simulations were performed using the program EasySpin.[37]

X-ray Crystallographic Data Collection and Structure Determination. Crystallographic data were measured at the Molecular Structure Laboratory of the Chemistry Department of the University of Wisconsin–Madison. Suitable crystals of **4** and **5** were selected under oil and ambient conditions. For **4**, a purple block shaped crystal with dimensions 0.728 x 0.374 x 0.216 mm^3 was selected, and for **5** a purple plate crystal with dimensions 0.166 x 0.155 x 0.094 mm^3 was chosen. The crystals were attached to the tip of a MiTeGen MicroMount©, mounted in a stream of cold nitrogen at 100(1) K, and centered in the X-ray beam using a video monitoring system. The crystal evaluation and data collection were performed on a Bruker Quazar SMART APEX-II diffractometer with Mo-Kα ($\lambda = 0.71073$ Å) radiation. The data were collected using a routine to survey the reciprocal space to the extent of a full sphere to a resolution of 0.70 Å for **4** and 0.80 Å for **5** and were indexed by the APEX program.[38] The structures were solved via direct methods and refined by iterative cycles of least-squares refinement on F^2 followed by difference Fourier synthesis. All hydrogen atoms were included in the final structure factor calculation at idealized positions and were allowed to ride on the neighboring atoms with relative isotropic displacement coefficients. Absorption corrections were based on a fitted function to the empirical transmission surface as sampled by multiple equivalent measurements.[39] The systematic absences in the diffraction data were uniquely consistent with the space groups $P2_1/c$ for **4** and $P2_1/n$ for **5**, yielding chemically reasonable and computationally stable results of refinement, and both structures were solved using direct methods using XS software.[40] Compound **4** is a pseudo-merohedral twin with a twin component ratio of 54:46. The twin components are related by a 180° rotation about [1 0 0]. Compound **5** is a non-merohedral twin with a twin component ratio of 60:40. The twin components are related by 180° a rotation about [0 0 1].

ASSOCIATED CONTENT.

MALDI-MS and EPR spectra and simulations for **2** and **5**; crystallographic data for **4** and **5**, including tables for selected bond distances and angles; $^{31}P\{^1H\}$ NMR and ESI data for formation of $^{(18)}OPPh_3$. The Supporting Information is available free of charge via the Internet at http://pubs.acs.org.

AUTHOR INFORMATION.

Corresponding Author

*Email: berry@chem.wisc.edu

Current Address

‡ MTA Centre for Energy Research, Surface Chemistry, and Catalysis Department, PO Box 49, H-1525 Budapest, Hungary.

Notes

The authors declare no competing financial interests.

ACKNOWLEDGEMENTS.

We thank the U.S. Department of Energy, Chemical Sciences, Geosciences, and Biosciences Division, Office of Basic Energy Sciences, Office of Science (DE-FG02-10ER16204). A.R.C. thanks the National Science Foundation for a Graduate Research Fellowship (DGE-0718123). NMR and EPR facilities at UW-Madison are supported by the NSF (CHE-1048642 and CHE-0741901, respectively), and mass spectrometry instruments are funded by NIH (1S10 OD020022-1 and NCRR 1S10RR024601-01). We thank Dr. Ilia Guzei for crystallographic insights and Dr. Linghong Zhang for assistance with GC-MS measurements.

REFERENCES.

(1) (a) Yoon, T. P.; Ischay, M. A.; Du, J. *Nat. Chem.* **2010**, *2*, 527. (b) Prier, C. K.; Rankic, D. A.; MacMillan, D. W. C. *Chem. Rev.* **2013**, *113*, 5322.
(2) (a) Pap, J. S.; DeBeer George, S.; Berry, J. F. *Angew. Chem. Int. Ed.* **2008**, *47*, 10102. (b) Long, A. K. M.; Yu, R. P.; Timmer, G. H.; Berry, J. F. *J. Am. Chem. Soc.* **2010**, *132*, 12228. (c)

Long, A. K. M.; Timmer, G. H.; Pap, J. S.; Snyder, J. L.; Yu, R. P.; Berry, J. F. *J. Am. Chem. Soc.* **2011**, *133*, 13138. (d) Corcos, A. R.; Long, A. K. M.; Guzei, I. A.; Berry, J. F. *Eur. J. Inorg. Chem.* **2013**, 3808.

(3) (a) Schlangen, M.; Neugebauer, J.; Reiher, M.; Schröder, D.; López, J. P.; Haryono, M.; Heinemann, F. W.; Grohmann, A.; Schwarz, H. *J. Am. Chem. Soc.* **2008**, *130*, 4285. (b) Izzet, G.; Ishow, E.; Delaire, J.; Afonso, C.; Tabet, J. C.; Proust, A. *Inorg. Chem.* **2009**, *48*, 11865. (c) Scepaniak, J. J.; Young, J. A.; Bontchev, R. P.; Smith, J. M. *Angew. Chem. Int. Ed.* **2009**, *48*, 3158. (d) Schöffel, J.; Rogachev, A. Y.; DeBeer George, S.; Burger, P. *Angew. Chem. Int. Ed.* **2009**, *48*, 4734. (e) Hojilla Atienza, C. C.; Bowman, A. C.; Lobkovsky, E.; Chirik, P. J. *J. Am. Chem. Soc.* **2010**, *132*, 16343. (f) Thomson, R. K.; Cantat, T.; Scott, B. L.; Morris, D. E.; Batista, E. R.; Kiplinger, J. L. *Na.t Chem.* **2010**, *2*, 723. (g) Scheibel, M. G.; Askevold, B.; Heinemann, F. W.; Reijerse, E. J.; de Bruin, B.; Schneider, S. *Nat. Chem.* **2012**, *4*, 552. (h) Scheibel, M. G.; Wu, Y.; Stückl, A. C.; Krause, L.; Carl, E.; Stalke, D.; de Bruin, B.; Schneider, S. *J. Am. Chem. Soc.* **2013**, *135*, 17719. (i) Torres-Alacan, J.; Das, U.; Filippou, A. C.; Vöhringer, P. *Angew. Chem. Int. Ed.* **2013**, *52*, 12833. (j) Zolnhofer, E. M.; Käß, M.; Khusniyarov, M. M.; Heinemann, F. W.; Maron, L.; van Gastel, M.; Bill, E.; Meyer, K. *J. Am. Chem. Soc.* **2014**, *136*, 15072. (k) Sieh, D.; Burger, P. *Z. Anorg. Allg. Chem.* **2015**, *641*, 52. (l) Vreeken, V.; Siegler, M. A.; de Bruin, B.; Reek, J. N. H.; Lutz, M.; van der Vlugt, J. I. *Angew. Chem. Int. Ed.* **2015**, *54*, 7055. (m) Abbenseth, J.; Finger, M.; Wurtele, C.; Kasanmascheff, M.; Schneider, S. *Inorg. Chem. Frontiers* **2016**, *3*, 469. (n) Camp, C.; Grant, L. N.; Bergman, R. G.; Arnold, J. *Chem. Commun.* **2016**, *52*, 5538.

(4) (a) Smith, J. M. *Prog. Inorg. Chem.* **2014**, *58*, 417. (b) Berry, J. F. *Comments Inorg. Chem.* **2009**, *30*, 28.

(5) (a) Nugent, W. A.; Mayer, J. M. *Metal-Ligand Multiple Bonds*; John Wiley & Sons: New York, 1988. . (b) Yin, G. *Coord. Chem. Rev.* **2010**, *254*, 1826. (c) Winkler, J. R.; Gray, H. B. In *Molecular Electronic Structures of Transition Metal Complexes I*; Mingos, D. M. P., Day, P., Dahl, J. P., Eds.; Springer Berlin Heidelberg: 2012; Vol. 142, p 17. (d) Ray, K.; Heims, F.; Pfaff, F. F. *Eur. J. Inorg. Chem.* **2013**, *2013*, 3784. (e) Chen, Z.; Yin, G. *Chem. Soc. Rev.* **2015**, *44*, 1083. (f) Ray, K.; Heims, F.; Schwalbe, M.; Nam, W. *Curr. Opin. Chem. Biol.* **2015**, *25*, 159.

(6) (a) Moyer, B. A.; Meyer, T. J. *J. Am. Chem. Soc.* **1978**, *100*, 3601. (b) Moyer, B. A.; Meyer, T. J. *Inorg. Chem.* **1981**, *20*, 436. (c) Che, C.-M.; Wong, K.-Y.; Mak, T. C. W. *J. Chem. Soc., Chem. Commun.* **1985**, 546. (d) Che, C.-M.; Wong, K.-Y.; Mak, T. C. W. *J. Chem. Soc., Chem. Commun.* **1985**, 988. (e) Che, C. M.; Lai, T. F.; Wong, K. Y. *Inorg. Chem.* **1987**, *26*, 2289. (f) Che, C.-M.; Tang, W.-T.; Lee, W.-O.; Wong, W.-T.; Lai, T.-F. *J. Chem. Soc., Dalton Trans.* **1989**, 2011. (g) Che, C. M.; Tang, W. T.; Wong, W. T.; Lai, T. F. *J. Am. Chem. Soc.* **1989**, *111*, 9048. (h) Dengel, A. C.; Griffith, W. P.; O'Mahoney, C. A.; Williams, D. J. *J. Chem. Soc., Chem. Commun.* **1989**, 1720. (i) Nagao, H.; Nishimura, H.; Kitanaka, Y.; Howell, F. S.; Mukaida, M.; Kakihana, H. *Inorg. Chem.* **1990**, *29*, 1693. (j) Power, J. M.; Evertz, K.; Henling, L.; Marsh, R.; Schaefer, W. P.; Labinger, J. A.; Bercaw, J. E. *Inorg. Chem.* **1990**, *29*, 5058. (k) de Souza, V. R.; Nunes, G. S.; Rocha, R. C.; Toma, H. E. *Inorg. Chim. Acta* **2003**, *348*, 50. (l) Huynh, M. H. V.; Meyer, T. J. *Chem. Rev.* **2007**, *107*, 5004. (m) Gagliardi, C. J.; Westlake, B. C.; Kent, C. A.; Paul, J. J.; Papanikolas, J. M.; Meyer, T. J. *Coord. Chem. Rev.* **2010**, *254*, 2459. (n) Warren, J. J.; Tronic, T. A.; Mayer, J. M. *Chem. Rev.* **2010**, *110*, 6961.

(7) Man, W.-L.; Lam, W. W. Y.; Wong, W.-Y.; Lau, T.-C. *J. Am. Chem. Soc.* **2006**, *128*, 14669.

(8) Wong, K.-Y.; Che, C.-M.; Yip, W.-H.; Wang, R.-J.; Mak, T. C. W. *J. Chem. Soc., Dalton Trans.* **1992**, 1417.

(9) (a) Suslick, K. S.; Acholla, F. V.; Cook, B. R. *J. Am. Chem. Soc.* **1987**, *109*, 2818. (b) Suslick, K. S.; Watson, R. A. *Inorg. Chem.* **1991**, *30*, 912.
(10) Kunkely, H.; Vogler, A. *J. Am. Chem. Soc.* **1995**, *117*, 540.
(11) (a) Harischandra, D. N.; Zhang, R.; Newcomb, M. *J. Am. Chem. Soc.* **2005**, *127*, 13776. (b) Zhang, R.; Newcomb, M. *Acc. Chem. Res.* **2008**, *41*, 468. (c) Zhang, R.; Vanover, E.; Luo, W.; Newcomb, M. *Dalton Trans.* **2014**, *43*, 8749.
(12) Cheng, M.; Bakac, A. *J. Am. Chem. Soc.* **2008**, *130*, 5600.
(13) (a) Nippe, M.; Goodman, S. M.; Fry, C. G.; Berry, J. F. *J. Am. Chem. Soc.* **2011**, *133*, 2856. (b) Brogden, D. W.; Turov, Y.; Nippe, M.; Li Manni, G.; Hillard, E. A.; Clérac, R.; Gagliardi, L.; Berry, J. F. *Inorg. Chem.* **2014**, *53*, 4777. (c) Brogden, D. W.; Berry, J. F. *Chem. Commun.* **2015**, *51*, 9153.
(14) Villalobos, L.; Barker Paredes, J. E.; Cao, Z.; Ren, T. *Inorg. Chem.* **2013**, *52*, 12545.
(15) Goberna-Ferrón, S.; Peña, B.; Soriano-López, J.; Carbó, J. J.; Zhao, H.; Poblet, J. M.; Dunbar, K. R.; Galán-Mascarós, J. R. *J. Catal.* **2014**, *315*, 25.
(16) Ring, S.; Meijer, A. J. H. M.; Patmore, N. J. *Polyhedron* **2016**, *103*, 87.
(17) Xu, G.-L.; Jablonski, C. G.; Ren, T. *Inorg. Chim. Acta* **2003**, *343*, 387.
(18) Dunlop, K.; Wang, R.; Stanley Cameron, T.; Aquino, M. A. S. *J. Mol. Struct.* **2014**, *1058*, 122.
(19) (a) Lever, A. B. P.; Mantovani, E.; Ramaswamy, B. S. *Can. J. Chem.* **1971**, *49*, 1957. (b) Nakamoto, K. *Infrared and Raman Spectra of Inorganic and Coordination Compounds. Part B: Applications in Coordination, Organometallic, and Bioinorganic Chemistry*; 5th ed.; John Wiley & Sons: New York, 1997.
(20) Crystallographic data for $Ru_2(DPhF)_4(NO_3)$: space group = $C2/c$; unit cell dimensions a = 14.028 Å; b = 13.571 Å; c = 23.189 Å; β = 91.33°; Vol = 4413.60 $Å^3$.
(21) Gowda, N. M. N.; Naikar, S. B.; Reddy, G. K. N. In *Advances in Inorganic Chemistry*; Emeleus, H. J., Sharpe, A. G., Eds.; Academic Press: 1984; Vol. Volume 28, p 255.
(22) Chakravarty, A. R.; Cotton, F. A.; Tocher, D. A. *Inorg. Chem.* **1985**, *24*, 1263.
(23) Bond distances and angles for minor component (8.82%) of another Ru(1) atom not reported here.
(24) Based on a search of the Cambridge Structural Database.
(25) Cherin, P.; Hamilton, W. C.; Post, B. *Acta Cryst.* **1967**, *23*, 455.
(26) (a) Lin, C.; Ren, T.; Valente, E. J.; Zubkowski, J. D.; Smith, E. T. *Chem. Lett.* **1997**, *26*, 753. (b) Bear, J. L.; Han, B.; Huang, S.; Kadish, K. M. *Inorg. Chem.* **1996**, *35*, 3012. (c) Kadish, K. M.; Garcia, R.; Phan, T.; Wellhoff, J.; Van Caemelbecke, E.; Bear, J. L. *Inorg. Chem.* **2008**, *47*, 11423. (d) Pap, J. S.; Snyder, J. L.; Piccoli, P. M. B.; Berry, J. F. *Inorg. Chem.* **2009**, *48*, 9846.
(27) Connelly, N. G.; Geiger, W. E. *Chem. Rev.* **1996**, *96*, 877.
(28) Chakravarty, A. R.; Cotton, F. A.; Tocher, D. A.; Tocher, J. H. *Polyhedron* **1985**, *4*, 1475.
(29) (a) Berry, J. F.; Bill, E.; Bothe, E.; George, S. D.; Mienert, B.; Neese, F.; Wieghardt, K. *Science* **2006**, *312*, 1937. (b) Chen, T.-H.; Asiri, N.; Kwong, K. W.; Malone, J.; Zhang, R. *Chem. Commun.* **2015**, *51*, 9949.
(30) (a) The corresponding Ru–Ru≡N complex has been shown unambiguously to have an S = 1/2 ground state with an unpaired electron in the Ru–Ru δ* orbital.[2] The addition of one more electron upon changing N to O is therefore expected to fill the δ* level yielding a diamagnetic ground state. (b) DFT calculations comparing $Ru_2(chp)_4O$ (**6**) in both singlet and triplet ground states were performed here. Results from both the BP86 and B3LYP functionals are in

agreement that the favored electronic ground state for **6** is the singlet state. See SI for computational details.

(31) (a) Atkins, P. W.; Symons, M. C. R. *J. Chem. Soc.* **1962**, 4794. (b) Livingston, R.; Zeldes, H. *J. Chem. Phys.* **1964**, *41*, 4011. (c) Wertz, J. E.; Bolton, J. R. In *Electron Spin Resonance: Elementary Theory and Practical Applications*; Chapman and Hall: New York, 1986, p 164.

(32) (a) Rotlevi, E.; Treinin, A. *J. Phys. Chem.* **1965**, *69*, 2645. (b) Svoboda, O.; Kubelová, L.; Slavíček, P. *J. Phys. Chem. A* **2013**, *117*, 12868.

(33) (a) Madsen, D.; Larsen, J.; Jensen, S. K.; Keiding, S. R.; Thøgersen, J. *J. Am. Chem. Soc.* **2003**, *125*, 15571. (b) Thøgersen, J.; Gadegaard, A.; Nielsen, J.; Jensen, S. K.; Petersen, C.; Keiding, S. R. *J. Phys. Chem. A* **2009**, *113*, 10488.

(34) Brown, T. R.; Dolinar, B. S.; Hillard, E. A.; Clérac, R.; Berry, J. F. *Inorg. Chem.* **2015**, *54*, 8571.

(35) Lutterman, D. A.; Degtyareva, N. N.; Johnston, D. H.; Gallucci, J. C.; Eglin, J. L.; Turro, C. *Inorg. Chem.* **2005**, *44*, 5388.

(36) Lin, C.; Ren, T.; Valente, E. J.; Zubkowski, J. D.; Smith, E. T. *Chem. Lett.* **1997**, *26*, 753.

(37) Stoll, S.; Schweiger, A. *J. Magn. Reson.* **2006**, *178*, 42.

(38) APEX2 2014.

(39) (a) SADABS 2014/5. (b) TWINABS 2012/1.

(40) XS 2013/1.

TOC GRAPHIC.